Cycle-by-cycle analysis of neural oscillations

Scott Cole[1], Bradley Voytek*[1,2,3]
[1]Neurosciences Graduate Program, [2]Department of Cognitive Science, [3]Halıcıoğlu Data Science Institute, University of California, San Diego

Corresponding author:
Dr. Bradley Voytek
Department of Cognitive Science
University of California, San Diego
9500 Gilman Dr.
La Jolla, CA 92093-0515
Tel: 858-534-0002
email: bvoytek@ucsd.edu

Abstract

Neural oscillations are widely studied using methods based on the Fourier transform, which models data as sums of sinusoids. This has successfully uncovered numerous links between oscillations and cognition or disease. However, neural data are nonsinusoidal, and these nonsinusoidal features are increasingly linked to a variety of behavioral and cognitive states, pathophysiology, and underlying neuronal circuit properties. Here, we present a new analysis framework—one that is complementary to existing Fourier- and Hilbert-transform based approaches—that quantifies oscillatory features in the time domain, on a cycle-by-cycle basis. We have released this cycle-by-cycle analysis suite as *bycycle*, a fully documented, open-source Python package with detailed tutorials and troubleshooting cases. This approach performs tests to assess whether an oscillation is present at any given moment and, if so, quantifies each oscillatory cycle by its amplitude, period, and waveform symmetry, the latter of which is missed using conventional approaches. In a series of simulated event-related studies, we show how conventional Fourier- and Hilbert-transform approaches can conflate event-related changes in oscillation burst duration as increased oscillatory amplitude and as a change in the oscillation frequency, even though those features were unchanged in simulation. Our approach avoids these errors. Further, we validate this approach in simulation and against experimental recordings of patients with Parkinson's disease, who are known to have nonsinusoidal beta (12-30 Hz) oscillations.

New and Noteworthy

We introduce a fully documented, open-source Python package, *bycycle*, for analyzing neural oscillations on a cycle-by-cycle basis. This approach is complementary to traditional, Fourier- and Hilbert-transform based approaches, but avoids specific pitfalls. First, *bycycle* confirms an oscillation is present, to avoid analyzing aperiodic, non-oscillatory data as oscillations. Next, it quantifies nonsinusoidal aspects of oscillations, increasingly linked to neural circuit physiology, behavioral states, and diseases. This approach is tested against simulated and real data.

Introduction

As a prominent feature of brain recordings, neural oscillations are frequently correlated to both pathologies (Uhlhaas and Singer 2010; Voytek and Knight 2015) and healthy behaviors such as movement, sleep, perception, and cognitive performance (Klimesch 1999; Massimini et al. 2004; Hanslmayr et al. 2007; Miller et al. 2007). Standard approaches for studying these oscillations are based on the Fourier transform, which decomposes a signal into component stationary sinusoids. However, brain rhythms are neither strictly stationary nor sinusoidal, as they come and go with varying amplitudes, frequencies, and waveforms (van Dijk et al. 2010; Jones 2016; Cole and Voytek 2017; Schaworonkow and Nikulin 2018). Therefore, decomposition of the neural signal using the Fourier transform does not parsimoniously capture all of the interesting structure present in neural signals. This is suboptimal given that nonsinusoidal oscillatory features carry physiological information (Buzsáki et al. 1986; Hentschke et al. 2007; Pietersen et al. 2009; Mazaheri and Jensen 2010; Belluscio et al. 2012; Lewis et al. 2012; Lee and Jones 2013; Trimper et al. 2014; Sherman et al. 2016; Cole and Voytek 2017; Cole et al. 2017; Bartz et al. 2018, Jackson et al., 2019), and non-stationarities of low-frequency cortical oscillations may reflect different physiological processes (Peterson and Voytek 2017; Cole and Voytek 2018). Not properly accounting for these nonsinusoidal waveforms makes conventional analyses susceptible to artifactual results, such as apparent phase-amplitude and cross-frequency coupling where no such multi-frequency interaction exists (Kramer et al. 2008; Gerber et al. 2016; Lozano-Soldevilla et al. 2016; Scheffer-Teixeira and Tort 2016; Cole et al. 2017; Vaz et al. 2017).

Methods used to analyze temporal properties of oscillations are also usually based on the Fourier- and Hilbert-transforms. “Instantaneous” measures of oscillatory amplitude and frequency are widely used to estimate these time-varying properties of an oscillation of interest (Canolty et al. 2006; Voytek et al., 2013; Voytek et al., 2015; Samaha and Postle 2015). However, the computation of such instantaneous features does not directly measure them in the original recording. Instead values are imputed from a transformed version of the data in which the signal is usually limited to a narrow sinusoidal frequency band (Bruns 2004). The mathematical nature of these approaches is such that they will always give a numerical result; they will always return an instantaneous amplitude, phase, and frequency value, even if there is no oscillation present in the signal (Haller et al., 2018). This is nonoptimal because amplitude, phase, and frequency—as they are often intuited—should be undefined if no oscillation is present. To address the issue of identifying periods of oscillation versus no oscillation, new methods, such as delay differential analysis, have been developed to identify rhythmic sections of the signal in which oscillatory analysis is warranted (Sampson et al., 2019). Periods of no oscillations are common because aggregate electrophysiological signals such as EEG, MEG, ECoG, and LFP contain an aperiodic component (Haller et al., 2018) that likely reflects the relative contributions of synaptic currents near the recorded region (Mazzoni et al., 2015; Gao et al., 2017). This means that narrowband analyses—without consideration of the nonstationary dynamics of the oscillatory signal—can give misleading results. This can lead to mischaracterizations of the data, such as phase slips, oscillatory frequency fluctuating within a single cycle, or an apparent increase in high frequency amplitude caused by a sharp transient (Kramer et al. 2008; Nelli et al. 2017).

We recently reviewed that waveform shape is diverse across the brain and relates to physiology, pathology, and behavior (Cole and Voytek 2017). The hippocampal theta rhythm (Buzsáki et al. 1985), cortical slow oscillation (Amzica and Steriade 1998), and the mu rhythm (Pfurtscheller et al. 1997) are particularly known to have stereotyped nonsinusoidal waveforms. There are a wide variety of circuit activation patterns for oscillators of each frequency (Womelsdorf et al. 2014), and the specifics of these dynamics may relate to the temporal dynamics of a single cycle of the recorded oscillation, or its waveform shape. Therefore, differences in waveform shape may hint at differences in the parameters, conditions, or even qualitative mechanisms of the oscillatory generator. One potential interpretation of waveform shape is that sharper oscillatory extrema may be produced by more synchronous neural activity (Sherman et al. 2016; Cole et al. 2017). This may be caused by excitatory synaptic currents occurring relatively simultaneously in a cortical region and integrating in the local field to yield a sharp waveform, whereas those same currents, more spread out in time, will result in a smoother local field potential.

Here we present a time-domain approach, complementary to traditional frequency-domain analyses, designed to characterize nonsinusoidal and transient brain rhythms to help quantify information not easily extracted from conventional, Fourier-based neural signal processing. For each oscillatory cycle, amplitude and period (frequency) are quantified, as are its waveform (a)symmetries. In contrast to the instantaneous features cited above, cycle-by-cycle measures are directly computed on points of the time series rather than relying on transforms that assume a quasi-sinusoidal structure. The only reliance on more traditional approaches is an initial, very broad filter used to remove the influence of high frequency, noisy transients on estimating lower frequency oscillation peaks and troughs. This is followed by a more narrow filter to isolate the oscillatory band of interest, solely for the purpose of finding zero-crossings. While these filters are used as simple tools to aid in segmenting the signal into cycles and localizing peaks, troughs, and zero-crossings, these filters do not significantly bias the waveform of the oscillation of interest. Importantly, the output also specifies whether the oscillation of interest is present or

absent in the signal during each “cycle” period, as it is unlikely that the oscillation is present throughout the whole duration of the signal (Fransen et al. 2015; Jones 2016). This is critical, as estimates of oscillatory features are meaningless if no oscillation is present (Haller et al., 2018).

Materials and Methods

All methods described here are available in the open-source package “bycycle”, available at https://github.com/bycycle-tools/bycycle, with detailed tutorials at https://bycycle-tools.github.io. All Python code to replicate the figures in this paper are shared at https://github.com/voytekresearch/Cole_2018_cyclebycycle. Filtering and Hilbert analyses, and signal simulations, made use of the neurodsp package (Cole et al., 2019). All tests are nonparametric, such that two-sample unpaired tests are Mann-Whitney U and two-sample paired tests are Wilcoxon Signed Rank.

Segmentation of signal into cycles

The first step in characterizing individual oscillatory cycles in a neural signal is to segment the entire recording into cycles. First, putative peaks and troughs are identified throughout the recording. The raw data (Fig. 1*A*) is passed through a lowpass filter to reduce higher frequency activity (Fig. 1*B*) that may interfere with peak and trough identification. Next, the signal is bandpass filtered around the oscillation band of interest, ideally verified from the power spectral density (Haller et al. 2018). The time points of the rise and decay zero-crossings are identified (Fig. 1*C*) and the minima and maxima between these zero-crossings are declared as putative peaks and troughs from the broadly-filtered (not narrowband filtered) signal (Fig. 1*D*). Finally, the midpoints of the rise and decay flanks are computed by finding the time point at which the voltage is halfway between the peak and trough voltage (Fig. 1*E*).

Together, the times of the extrema and flank midpoints can be used to estimate a “waveform phase” time series by linearly interpolating between their theoretical phases (Siapas et al. 2005). This means that between each extremum and zero-crossing, phase is assumed to be linear. For example, because the phase of a peak is 0 and the phase of the next zero-crossing is π/2, if there are 10 time-points between a peak and the next zero-crossing, then the phase of each time point between will increase in π/20 increments. If the signal is nonsinusoidal, this estimate slightly but systematically deviates from the instantaneous phase commonly computed by bandpass filtering the signal in the oscillatory frequency band and applying the Hilbert transform. This is because the Hilbert transform can artificially shift phase values in an attempt to fit a sinusoid to a nonsinusoidal signal. This can cause non-intuitive phase shifts, for example fitting sinusoidal peaks away from the true time domain voltage peak for that cycle. That is, the waveform phase estimate more closely matches the locations of the oscillatory peaks and troughs, which can be skewed when a nonsinusoidal oscillation is filtered in a narrow frequency band (Belluscio et al. 2012; Dvorak and Fenton 2014).

Note that this process of cycle segmentation uses some bandpass filtering for localizing extrema (Fig. 1*B,C*). This superficially seems in contrast with a proclaimed key advantage of the cycle-by-cycle method, where a sinusoidal waveform is not assumed. However, individual cycle statistics are not computed on this narrowband filtered signal; filtering here is a tool useful for roughly estimating peak and trough times. The lowpass filter is used to remove the high frequencies that may make identifying the peaks and troughs of the lower frequency rhythm more difficult. However, the filter is potentially removing some of the oscillatory signal that is especially sharp and requires high-frequency sine waves to reconstruct. Therefore, the cutoff frequency of the lowpass filter is set to around 4 times the frequency of the oscillations of interest (e.g., 40 Hz for ~10 Hz alpha oscillations) as a compromise between the fidelity of waveform shape and the ability to localize peaks and troughs (Fig. 1*A*-*B*).

Cycle feature computation

After the signal is segmented into cycles, each cycle is characterized by a few intuitive features (Fig. 1*F*). In all analyses, cycles are chosen to start and end at consecutive troughs. The amplitude of the cycle is computed as the average voltage difference between the peak and the two adjacent troughs. The period is defined as the time between the two troughs. Rise-decay symmetry (rdsym) is the fraction of the period that was composed of the rise time. A rise-decay symmetry value of 0.5 would therefore indicate the cycle had equal durations of rise and decay. Note that while a sinusoid has rdsym=0.5, several classes of nonsinusoids can as well, such as triangle waves.

Peak-trough symmetry (ptsym) is the fraction of the period, encompassing the previous trough and current peak, that was composed of the peak. Similar to rise-decay symmetry, a peak-trough symmetry value of 0.5 indicates that the peak and trough were the same duration. The peak period is defined as the time between a rise midpoint and subsequent decay midpoint, while the trough period is defined as the time between a decay midpoint and subsequent rise midpoint. The values of each cycle feature are provided in a table in which each row represents an individual cycle. Fig. 1*G* shows the cycle feature values for the recording processed throughout Fig. 1. The distributions of these features across all cycles can be computed to compare oscillation properties in different neural signals (Fig. 2*G-J*).

Detection of oscillatory periods

After segmenting the signal into putative cycles, an algorithm is applied to determine whether each cycle is part of an oscillatory rhythm in the signal. The entire signal is preliminarily segmented into putative cycles, even the portions in which no oscillation is present. Therefore, the term “cycle” is used here not to specifically refer to a cycle of an oscillatory process, but rather a time segment lasting approximately one period of the oscillation of interest. Oscillation presence is identified by time periods in which at least three consecutive putative cycles in the time series had similar amplitudes, similar periods, and rise and decay flanks that are predominantly monotonic. To test this, three additional features are computed for each cycle. First, the amplitude consistency of a cycle is quantified as the relative difference in the rise and decay voltage (e.g., 0.5 corresponds to the change in voltage in one flank being 2 times bigger than the other, 1.0 corresponds to the rise and decay flanks having equal changes in voltage, etc.). The minimum value is taken after computing this measure for each pair of adjacent rise and decay flanks that includes one of the current cycle’s flanks. The period consistency feature is computed as the maximal relative difference between the cycle’s period and the period of the adjacent cycles (e.g., 0.5 corresponds to the previous or subsequent period being twice or half the duration of the current cycle). The third and final feature, monotonicity, is the fraction of instantaneous voltage changes (difference between consecutive samples) that are positive during the rise phase and negative during the decay phase (e.g., 0.8 corresponds to 20% of the voltage time series going in the opposite direction of the current flank).

These requirements for declaring oscillation presence are based on the definition of a periodic process, in which the voltage at time t + □ should be predictable from the voltage at time t, where the process has a period □. In order for the future voltage to be reliably predicted from the past voltage, the amplitude and period must be conserved from cycle to cycle. The monotonicity requirement was added because it was empirically found to separate periods of apparent periodic and aperiodic activity.

For all simulated recordings, amplitude consistency and period consistency thresholds were set to 0.6 and the monotonicity threshold was set to 0.9, because visual inspection of the

oscillations detection results showed that these parameters detected oscillations well. For the motor cortical beta recordings, oscillation detection parameters were tuned to improve accuracy as judged by visual inspection (amplitude consistency threshold = 0.3, period consistency threshold = 0.5, monotonicity threshold = 0.6). This was necessary because the beta oscillations were generally less monotonic and less consistent compared to the simulated data. An additional threshold was added such that cycle amplitude must be above the twentieth percentile to avoid aperiodic portions of the signal being considered as a part of an oscillation.

Simulation of oscillations with noise

Voltage time series were simulated using the neurodsp package (Cole et al., 2019) to have properties similar to real neural recordings. Four sets of signals were simulated for Figs. 2-5. Unless otherwise specified, the oscillation in these simulated signals was in the alpha range (6-14 Hz) with an average frequency of 10 Hz.

The nonstationary, nonsinusoidal oscillatory signal was simulated as follows:

1. A time-series of zeroes is created to match the desired length of the ultimate signal.
2. The zeroes time series is broken into windows representing “cycles” of a potential oscillation, where each window length is the period of the potential oscillation, drawn randomly from a normal distribution, here of mean 100 ms and standard deviation of 5 ms.
3. Each window is defined to be either in an oscillatory state or not. If the prior window is not in an oscillatory state, then the current window starts oscillating with a probability of 0.1.
4. Once an oscillating cycle occurs, each successive cycle will end the oscillatory state with a probability of 0.1. In other words, if the signal was currently in an oscillatory state, then it had a 10% probability of exiting that state after each cycle.
5. If a window is determined to be in an oscillatory state, a waveform is simulated as follows:
    a. The amplitude of that cycle is sampled from a distribution, here of mean 1 and standard deviation of 0.1 (arbitrary units).
    b. The rdsym of that cycle is sampled from a distribution, here of mean 0.5 and standard deviation of 0.05.

Noise was simulated using brown ($1/f^2$) noise that was highpass filtered at 1 Hz (filter order = 3 seconds). This brown noise is referred to as the “aperiodic” component of the signal, whereas the oscillation is referred to as the “periodic” component (Haller et al., 2018). This noise was added to the periodic oscillatory signal. Unless otherwise specified, the aperiodic component was scaled such that it had the same variance as the periodic component. A lowpass filter at 40 Hz (filter order = 100 ms) was applied prior to cycle-by-cycle analysis, in order to remove high frequency power that would complicate extrema localization.

To compare cycle feature distributions across recordings, two example recordings (Fig. 2*A,D*) were simulated using the parameters specified above, for 1000 seconds each. However, the second signal (Fig. 2*D*) was modified such that the power of the periodic component was twice that of the power of the aperiodic component, and the average rise-decay symmetry was 0.3 instead of 0.5. To determine the accuracy of the cycle features, 41 recordings were simulated for 5 minutes each in which the relative variance of the aperiodic and periodic components was varied between 0.1 and 10 with equal spacing in logarithmic space (Fig. 3). In this simulation, the standard deviations of cycle features were increased to □=0.2 for amplitude, □=15 ms for period, and □=0.1 for rise-decay symmetry.

Two additional sets of signals were simulated in order to compare cycle-by-cycle measures with instantaneous amplitude and frequency measures (Figs. 4,5). These simulations were modeled after an event-related design where each simulation is a “trial”. Trials were simulated such that a 10 Hz oscillation burst was induced after an “event”. Brown noise was simulated throughout the trial (-1 to 2 seconds), and a bursting oscillation was simulated from 0 to 2 seconds in the same manner as above. Three conditions of 100 trials each were simulated for assessing amplitude measures. The “higher amp” condition induced alpha oscillations with a 20% greater amplitude than in the “baseline” condition. The “more bursts” condition was 50% more likely to enter an oscillation and 50% less likely to leave an oscillation, compared to the other conditions. Similar trials were simulated for comparing cycle-by-cycle and instantaneous measures of frequency. For this experiment, a “faster” condition was simulated using an 11 Hz oscillation instead of a 10 Hz oscillation.

Instantaneous amplitude and frequency computation

Instantaneous measures of amplitude and frequency were computed using common methods and applied to the simulated alpha oscillations described in the previous paragraph. Signals were first bandpass filtered (8-12 Hz) and then the Hilbert transform was applied. The magnitude of the resultant time series was computed to obtain the instantaneous amplitude estimate, and the angle was computed to obtain the instantaneous phase estimate. Instantaneous frequency was computed from the instantaneous derivative of the phase time series, and then iteratively median filtered using 10 window sizes linearly spaced between 10 ms and 400 ms, as previously described (Samaha and Postle 2015).

Motor cortical beta recordings

Electrocorticography recordings from 23 patients with Parkinson’s disease were obtained during surgery for implantation of a deep brain stimulator and publicly released (de Hemptinne et al. 2015). Briefly, a strip of electrodes with 1 cm contacts was inserted over the primary motor cortex (M1) and re-referenced using a bipolar montage of adjacent contacts. The signals analyzed in this study were from a single channel in which one of the electrodes was over M1. Recordings were collected for 30 seconds before and during DBS. For more information on the data collection see (de Hemptinne et al. 2015). Recording sampling rate was 1000 Hz. Prior to cycle-by-cycle analysis, signals were lowpass filtered at 200 Hz, and high frequency peaks (60 Hz and above) were removed (for more information see (Cole et al. 2017)). During cycle segmentation the narrow bandpass filter cutoff frequencies were 13 and 30 Hz.

[Insert Figure 1 here]

Results

Comparison of cycle-by-cycle oscillatory feature distributions

To demonstrate the general approach of our method, we applied our cycle-by-cycle analysis technique (Fig. 1, see Methods) to two simulated neural recordings of 1000 seconds each. These simulated signals (Fig. 2*A,D*, “signal A” and “signal D”) are composed of both transient 10 Hz (alpha) oscillations (Fig. 2*B,E*) and aperiodic noise (Fig. 2*C,F*) (see Methods). Periods of the signal in which alpha oscillations were present were determined, and the features of these cycles were computed (see Methods). The distributions of each cycle feature were compared between the two signals. Signal D in general has higher amplitude alpha oscillations (mean peak-to-trough voltage = 3.0) compared to the signal A (mean 2.6) as shown in their histograms (Fig. 2*G*). This is because the two signals were simulated with different ratios of periodic to aperiodic power, prior to z-scoring. However, the two signals were not differentiated by their periods, which were both 100 ms on average (Fig. 2*H*). These signals were detected to have

differences in their rise-decay symmetry (Fig. 2*I*) but not peak-trough symmetry (Fig. 2*J*). This is because signal A was simulated to have an average rise-decay symmetry of 0.5 whereas signal D was simulated to have an average rise-decay symmetry of 0.3. However, the average measured rise-decay symmetry for signal D was 0.37. This is because adding noise to the data biased the symmetry measures such that they seem to be more symmetric.

[Insert Figure 2 here]

Accuracy of cycle-by-cycle characterization

To assess the accuracy of our cycle-by-cycle oscillatory characterization, we compared cycle features measured in simulated neural signals (5 minutes each) with the ground truth of the simulation. Signals were simulated at a variety of signal-to-noise (SNR) levels by controlling the relative power of the simulated periodic component ("oscillation", e.g. Fig. 2*B*) and the simulated aperiodic component ("noise", e.g. Fig. 2*C*). Example traces are plotted for an example signal with a high amount of noise (SNR = 0.32, Fig. 3*A*) and one with a lower amount of noise (SNR = 3.2, Fig. 3*B*). The gray trace is the simulated periodic component, and the black trace is the combination of the periodic and aperiodic components after a 40 Hz lowpass filter, applied to improve peak and trough localization. Sensibly, there is a greater correspondence between the simulated oscillations and the measured oscillation in the signal with higher SNR, as shown by the stronger correlation between gray and black traces in Fig. 3*B* compared to Fig. 3*A*.

The error between the measured amplitude, period, and rise-decay symmetry estimates of each cycle was computed for these signals. For the noisier signal (SNR = 0.32), there was larger variance between the measured cycle features and the ground truth. The correlations between the measurements and the ground truth were low for all cycle features, namely amplitude (Fig. 3*C*, Pearson r = 0.19), period (Fig. 3*D*, r = 0.25), and rise-decay symmetry (Fig. 3*E*, r = 0.06). For the signal with less noise (SNR = 3.2), the correlations were higher for amplitude (Fig. 3*F*, r = 0.52), period (Fig. 3*G*, r = 0.46), and rise-decay symmetry (Fig. 3*H*, r = 0.30). For each feature, the average error was computed across simulated signals with SNR varying from 0.1 to 10. The error of each cycle feature estimate was normalized by the ground truth in order to compute a normalized error measurement. Fig. 3*I* shows that this error decreases as signal SNR increases. Note that these errors are computed for individual cycles, but analyses are intended be performed on cycle feature averages over trials or resting-state recordings. In these cases, as more cycles are sampled, the error between the ground-truth and measured cycle feature means will decrease.

[Insert Figure 3 here]

Cycle-by-cycle estimates vs. instantaneous measures of amplitude and frequency

It is possible that estimating amplitude and frequency on a cycle-by-cycle basis could provide a more precise estimate of these properties compared to conventional "instantaneous" approaches that first apply a narrow bandpass filter, followed by the Hilbert transform. Here we compared how these measures could differentiate conditions in a simulated experiment that elicit oscillations with differing amplitude and frequency (see Methods). This hypothetical experiment resulted in a 10 Hz oscillation appearing after an event. There were three conditions: "baseline", "higher amp", and "more bursts" (Fig. 4*A*). The oscillations in the "higher amp" condition were 10% greater in amplitude than in the other conditions. The "more bursts" condition was 50% more likely to enter an oscillatory state and 50% less likely to leave it compared to the other conditions. Instantaneous and cycle-by-cycle amplitudes were computed for the simulated trials (100 per condition) and averaged across each condition.

The average instantaneous amplitude trace for “higher amp” was appropriately greater compared to the “baseline” condition (Fig. 4*B*). However, the instantaneous amplitude for the “more bursts” trials was even greater, even though the simulated oscillations were the same size as the “baseline” trials. This undesirable trait of conflating more (or longer) bursts as higher average amplitude is the result of averaging non-stationary processes across many trials (Latimer et al. 2015; Jones 2016). This means that, using traditional Hilbert approaches, a consistent oscillation at a lower amplitude may not be distinguishable from an inconsistent oscillation at a higher amplitude.

In contrast, the cycle-by-cycle amplitude measure was appropriately increased specifically only for the “higher amp” condition (red line, Fig. 4*C*). Additionally, the cycle-by-cycle approach quantifies how often the signal was in an oscillatory state, and so we can observe that the “more bursts” condition was oscillating more than the other two conditions (Fig. 4*D*). In this simulated experiment, the cycle-by-cycle measures better discriminate the appropriate features of oscillatory amplitude as compared to instantaneous methods.

Further, we examined how well these two approaches perform with regards to measuring oscillatory amplitude. To do this, amplitude was averaged from 500 to 1000 ms in each trial. Across trials, this mean instantaneous amplitude did not significantly differentiate the “baseline” and “higher amp” conditions (Fig. 4*E*, $U = 4480$, $p = 0.10$) while the mean cycle amplitude significantly differentiated these conditions (Fig. 4*F*, $U = 182$, $p < 10^{-5}$). Additionally, instantaneous amplitude analysis falsely resulted in a significant difference in oscillation amplitude between the “baseline” and “more bursts” conditions (Fig. 4*G*, $U = 2781$, $p < 10^{-7}$), while the cycle-by-cycle amplitude analysis successfully found no significant difference (Fig. 4*H*, $U = 819$, $p = 0.37$).

[Insert Figure 4 here]

Similarly, we simulated an experiment to determine the difference in the efficacy of oscillation frequency estimates obtained from the conventional instantaneous approach and the cycle-by-cycle approach (Fig. 5*A*). Rather than simulating a set of trials with increased amplitude, here a “faster” condition was added in which an 11 Hz oscillation was simulated, whereas the oscillations in the other conditions had a frequency of 10 Hz. The instantaneous frequency was averaged across trials for each condition (Fig. 5*B*). Similarly, frequency was computed from the cycle-by-cycle period measures and averaged across trials (Fig. 5*C*). Both instantaneous and cycle-by-cycle approaches were able to differentiate between the “baseline” and “faster” conditions (Fig. 5*D-E*, instantaneous $U = 3351$, $p < 10^{-4}$; cycle $U = 100$, $p < 10^{-7}$). However, the instantaneous frequency estimates were considerably lower than the simulated ground truth frequencies, such that the average instantaneous frequency for each trial was 9.3 Hz for the “baseline” condition and 9.9 Hz for the “faster” condition. In contrast, the cycle-by-cycle estimates of frequency were appropriately around 10 Hz for the “baseline” condition and 11 Hz for the “faster” condition.

Furthermore, there was a spurious increase in instantaneous frequency in the “more bursts” condition compared to the “baseline” condition (Fig. 5*F*, $U = 3389$, $p < 10^{-4}$). This again can be attributed to the fact that the instantaneous measures do not account for whether the oscillation is present in the signal, and so these estimates can be biased by aperiodic portions of the signal. These aperiodic portions of the signal will have an average frequency corresponding to the power-weighted average frequency component in the frequency band of interest (in this case alpha, 6-14 Hz). Like real neural signals, the power in these simulated signals decreases as a function of frequency, and so, the power-weighted average frequency during an aperiodic

segment would lie somewhere below 10 Hz, the midpoint of the defined oscillation frequency band of interest. This means that, using traditional Hilbert approaches, the prevalence of an oscillation may confound an apparent change in frequency. In contrast to the instantaneous frequency measure, there was no difference in the cycle-by-cycle frequency estimates measured in the “baseline” and “more bursts” conditions (Fig. 5*G*, U = 769, p = 0.45).

[Insert Figure 5 here]

Cycle-by-cycle analysis of motor cortical beta oscillations in Parkinson’s Disease

In addition to simulated data, we applied the cycle-by-cycle approach to analyze motor cortical electrocorticography recordings. We have previously shown that motor cortical beta oscillations are “sharper” in patients with Parkinson’s disease (Cole et al. 2017; Jackson et al. 2019), and that this sharpness is decreased with deep brain stimulation (DBS) treatment (Cole et al. 2017) or dopaminergic medication (Jackson et al. 2019). The current “peak-trough asymmetry” measure was designed to measure the same intuitive sense of “sharpness” reported in the previous studies, but it differs in that it is computed as a temporal ratio, as opposed to differences in voltages (Fig. 1*F*, see Methods). This new metric is used because the previously-used “sharpness asymmetry” intrinsically, and undesirably, scaled with amplitude.

Fig. 6*A*-*B* show recordings from an example subject before and during DBS. In this subject, DBS decreased the amplitude (Fig. 6*C*), and period (Fig. 6*D*), of beta oscillations, but did not affect their rise-decay symmetry (Fig. 6*E*). Across the patient population (N=23), there was no consistent effect of DBS on amplitude (Wilcoxon Signed Rank test, W = 84, p = 0.10), period (W = 90, p = 0.14), or rise-decay asymmetry (W = 102, p = 0.27). However, DBS did elongate the relative peak time in the example subject (Fig. 6*F*), and consistently caused the beta oscillations to become more peak-trough symmetric (Fig. 6*G*, W = 71, p = 0.019), consistent with the previously published sharpness ratio results (Cole et al. 2017). Note that peak-trough asymmetry here is measured as the difference from a symmetric oscillation, such that 0 represents equal duration peaks and troughs, and 0.1 represents an oscillation in which the average cycle was 60% peak or 60% trough (i.e., 0.6 - 0.5 = 0.1 and 0.4 - 0.5 = -0.1). This was done because the polarity was not consistent across recordings.

[Insert Figure 6 here]

Discussion

Here we have presented a novel framework and technique for analyzing the properties of oscillations in neural signals. This cycle-by-cycle analysis approach is complementary to, and offers advantages when used in addition to, conventional approaches based solely on the Fourier and Hilbert transforms. Our method offers an alternative, and arguably more intuitive, estimate of an oscillation’s amplitude and frequency on a cycle-by-cycle basis. These estimates are incorporated in the same framework that has previously been used to estimate rise-decay symmetry (Cole et al., 2017). We have expanded this framework to offer a novel peak-trough symmetry measure, which quantifies the “sharpness” of an oscillatory waveform. Using empirical recordings from human patients, we showed this symmetry measure differentiates between treatment conditions. Further, using simulated data we showed that our new amplitude and frequency estimates can be more sensitive and specific than conventional techniques.

This technique offers further analytic possibilities, beyond what is demonstrated in this paper. In addition to comparing distributions of cycle features from separate recordings (e.g., DBS on vs. DBS off), cycles can be analyzed in an event-related manner to examine the effects of task conditions or correlates to behavioral responses, such as reaction time, or physiological

features such as local spiking (Cole and Voytek, 2018). This framework additionally allows for studying the temporal dynamics by which oscillatory features change over time, similar to studies looking at changes to oscillatory power or frequency. Further, if a signal contains multiple oscillations of interest, then the analysis can be run multiple times using distinct frequency bands. Additionally, the oscillatory detection algorithm allows for quantifying features of oscillation presence, such as burst duration or burst rate, that may correlate meaningfully to experimental parameters.

Caveats of cycle-by-cycle analysis and comparisons to existing methods

Like Fourier-based analysis, there are also caveats of this cycle-by-cycle technique that need to be considered to minimize confounds. In a recent manuscript, we showed that cycle features are significantly autocorrelated for the rodent hippocampal theta rhythm (Cole and Voytek 2018). Because of this autocorrelation, it is therefore invalid to treat each cycle as independent in statistical tests. This is a similar caveat to trial-wise analyses, in which consecutive trials are often not independent. To bypass this issue and assess significance within a recording, the recording can be split into multiple non-overlapping segments, and a statistical test can be performed on a metric of each segment (e.g., mean difference in rdsym between conditions *A* and *B*).

It is also important to keep in mind that these cycle features are likely not independent of one another. For instance, the higher amplitude hippocampal theta rhythms tend to have shorter periods and are more rise-decay asymmetric and peak-trough asymmetric (Cole and Voytek 2018). Therefore, these features may capture physiologically redundant information. To tease apart some interdependencies, multiple features could be incorporated into a model to predict a condition or behavior of interest (e.g., general linear model or logistic regression), and the unique contribution of each feature can be assessed. For example, if oscillatory amplitude is greater in condition *A* vs. *B*, and amplitude is correlated with symmetry, then we will also observe that symmetry differs between conditions. However, a multidimensional model could detect whether symmetry contains any additional information beyond that provided by amplitude.

Because extrema localization is nontrivial, caution is necessary when performing analyses that consider the precise times of peaks and troughs. For example, an aperiodic process could delay the algorithm's trough localization, and so if a neuron fires most at the trough, it will appear that it fires at an earlier phase when the decay period is artificially elongated. However, a rat's position could be better decoded using extrema interpolation compared to the conventional Hilbert transform-based method (Belluscio et al. 2012). If it is difficult to filter the signal to achieve reasonable extrema localization and symmetry fidelity, then the oscillation may not be suitable for cycle-by-cycle analysis. For example, it is likely not reasonable to analyze the beta frequency band in the visual cortex because the presence of this rhythm is usually not evident in the time series, whereas alpha is prominent.

Hyperparameter selection is another notable challenge, but it is not a new one nor unique to oscillation parameterization. Setting thresholds for defining oscillation presence may require parameter tuning to achieve sensible classification. That said, visual inspection confirmed that the same hyperparameter settings worked reasonably across the simulations and experimental data analyzed here. Hyperparameters are not only present in the current method, but other oscillation detection methods benefit from tuning amplitude thresholds and filter lengths because they will significantly impact the results (Feingold et al. 2015). We recommend that the user runs the analysis with multiple hyperparameter choices to test the robustness of their results.

A key feature of the oscillation detection method used here is that it does not need to set an amplitude threshold to define oscillatory periods, as is the case for previously published algorithms for oscillatory burst detection (Hughes et al. 2012; Feingold et al. 2015; Watrous et al. 2017). This makes the current oscillation detection algorithm especially suitable for detecting oscillators that may occur at both small and large amplitudes, or that may vary greatly in stationarity between recordings. In contrast, using an amplitude threshold based on scaling the median oscillatory power (Feingold et al. 2015) inherently defines an upper limit on the fraction of the signal that can be classified as oscillatory. This may not be suitable, for example, in a set of hippocampal recordings in which theta oscillations can be present in more than 50% of the recording.

Other complementary tools exist for extracting information from neural signals that Fourier-based analyses do not concisely capture. Matching pursuit is a tool for decomposing a signal using a dictionary of functions, and has been used to analyze transient components of brain signals (Ray et al. 2003; Chandran et al. 2016). However, this approach has only so far been applied with a basis of Gaussian-modulated sinusoids, and it is nontrivial to decide how to parametrize the output to compare experimental conditions. Another approach, empirical mode decomposition (EMD), decomposes signals without forcing a basis function, such as the sinusoidal basis assumed in Fourier-based approaches (Liang et al. 2005; Pittman-Polletta et al. 2014). However, applications of EMD in neural signals have been limited by critical issues such as “mode mixing” in which an oscillation of interest is split among multiple components, and difficulty in identifying analogous components across different recordings (Park et al. 2013). More complicated methods have been developed to help partially overcome these issues, but EMD has rarely been applied to neural signals beyond providing features for machine learning algorithms (Diez et al. 2009; Orosco et al. 2009; Bajaj and Pachori 2012).

Few analysis techniques have been designed specifically for characterizing the time-domain waveform shape of brain oscillations. Characterizations of oscillation waveform shape have mostly been limited to locating peaks and troughs and quantifying the relative durations of rises and decays. In the hippocampal gamma oscillation, for example, the amplitude of a cycle is positively correlated with the period of the subsequent cycle, which has been interpreted as reflecting synaptic excitation being counterbalanced by proportional inhibition (Atallah and Scanziani 2009). The asymmetry of hippocampal theta oscillations have been characterized by the relative durations of the rise and decay periods, and is correlated to memory and spatial representation (Belluscio et al. 2012; Dvorak and Fenton 2014; Trimper et al. 2014; Amemiya and Redish 2018). Because of its notable asymmetry, researchers studying hippocampal theta have designed an alternative instantaneous phase estimate that involves identifying extrema in each cycle (Siapas et al. 2005; Belluscio et al. 2012). Additionally, two algorithms were recently developed to extract the waveform of the *prominent* oscillation in a neural signal (Gips et al. 2017; Jas et al. 2017), but these approaches do not capture changes in waveform shape within a recording.

Instantaneous and cycle-by-cycle measure comparison

In addition to its ability to quantify waveform symmetry, we believe that the cycle-by-cycle framework’s measures of amplitude and period also offer an advantage over current, widely-used methods for estimating instantaneous amplitude and frequency. An important step in computing instantaneous amplitude is convolution with a kernel of the frequency of interest. This means that the amplitude measure at any given point in time is actually computed using data from several cycles around that point (depending on the filter length). Because convolution is a linear operation, it is not specifically sensitive to oscillatory amplitude, but it will be strongly

biased by non-oscillatory sharp transients. Instantaneous frequency, derived from instantaneous phase, is similarly based on this convolution, and fluctuates within a cycle due to the cycle's temporal dynamics. However, when applied to a relatively stationary nonsinusoidal oscillation (e.g., hippocampal theta) this will cause fluctuating within-cycle frequency estimates, which do not actually reflect a change in the theta frequency, but rather reflects its sawtooth-like waveform. In addition, these approaches conflate periodic and aperiodic activity because every moment in the signal is assumed to represent an oscillation. As we demonstrated in simulation, conflating these two processes introduces noise. Perhaps an even more pernicious concern is one caused by the non-random, 1/f-like relationship between neural frequency and power, wherein event-related changes in the aperiodic signal—as has recently been demonstrated (Podvalny et al. 2015; Gao et al. 2017)—which can be mischaracterized as changes in instantaneous frequency.

In contrast to the widely used instantaneous measures, the time-resolved estimates of amplitude and period (frequency) using cycle-by-cycle estimates are more direct and intuitive measurements of the oscillation. Specifically, the amplitude measures the mean rise and decay voltages, and the period is computed as the time between consecutive peaks of a cycle in a putative oscillation. This method does not over-promise temporal resolution that it cannot reliably account for, and it is robust to issues that plague instantaneous measures such as sharp transients and nonsinusoidal waveforms. Additionally, we showed that the cycle-by-cycle measures of amplitude and frequency are more robust and better at differentiating these properties in simulated oscillations (Figs. 4,5). Specifically, instantaneous measures of both amplitude and frequency are biased by the proportion of the signal in which the oscillation is present, so this could underlie some past reports of changes in instantaneous amplitude and frequency.

There is some empirical precedence for analyzing individual cycles of brain rhythms. Adrian and Matthews (1934) studied the evolution of a gamma oscillation in response to injury to the cortex of a cat. Initially, they observed rhythmic transient discharges, which gradually became more frequent and broad, producing a more sinusoidal-like rhythm. They interpreted the initial transients as bursts of activity by a few local neurons, and that this activity spread out as the transient discharges merged into a quasi-sinusoid. Therefore, each cycle could be considered as a "packet" of neural activity that can be characterized distinctly from the previous and subsequent cycles using a cycle-by-cycle analysis framework. This view of each cycle as an informative physiological unit differs substantially from modern work on oscillations.

It is important to note that the specific methods and approaches we introduce here may not be the final *best* approaches, but they are a step toward more careful parameterization of the signals of interest. As we showed, without more careful parameterization, it is easy to conflate one physiological process—such as increased burst probability—with another entirely different process of oscillation amplitude change. Because our package is open source, the methods can be refined as new physiological data are collected, and as simulations are refined. For example, the cycle-detection approach introduced here is but one of many, and future studies may show that one approach performs best for one class of data, while a second approach performs best for another. Software modularity promotes flexibility in the light of new data. In addition, because we quantify how the *bycycle* approach is susceptible to noise, some low-pass filtering is necessary to balance time-domain extrema localization with noise transient confounding. Future approaches to denoise the data, perhaps through dynamic removal of the aperiodic signal, might prove more effective. Finally, although we only covered four cycle features in this paper (amplitude, period, rise-decay symmetry, and peak-trough symmetry), additional features can be designed and easily added to this workflow, such as monotonicity of the flanks or gamma

power (Lopes-Dos-Santos et al. 2018). This modularity is important because we do not know which features optimally characterize the physiology of waveforms. It is clear that no one feature is sufficient—for example rdsym=0.5 for both sinusoids and triangle waves—thus several cycle features are parameterized to better classify waveforms.

In summary, we have demonstrated a novel approach to analyzing neural oscillations using a cycle-by-cycle framework. This technique has advantages over conventional approaches that rely solely on Fourier-based techniques, including its ability to characterize oscillatory waveform symmetry and its inherent detection of whether an oscillation is present in the data or not. We additionally demonstrate its application on an experimental dataset of Parkinson's disease recordings and a simulated dataset with a simulated event-related alteration of alpha oscillation features. This method is well suited to analyze not only motor cortical beta rhythms, but any oscillation that is prominent in the raw data, such as the mu rhythm, visual cortical alpha, hippocampal theta, visual cortical gamma, thalamocortical spindles, cortical slow oscillation, and respiratory rhythms. While this open-source analysis framework is unique in its focus on oscillatory symmetry, it is also complementary to conventional analysis of oscillatory amplitude and period, and, as such, should be a standard part of the neural oscillation analysis toolbox.

References

Adrian ED, Matthews BH. The interpretation of potential waves in the cortex. J Physiol (Lond). 1934 Jul 31;81(4):440–71.

Amemiya S, Redish AD. Hippocampal Theta-Gamma Coupling Reflects State-Dependent Information Processing in Decision Making. Cell Rep. 2018 Mar 20;22(12):3328–38.

Amzica F, Steriade M. Electrophysiological correlates of sleep delta waves. Electroencephalogr Clin Neurophysiol. 1998 Aug;107(2):69–83.

Atallah BV, Scanziani M. Instantaneous modulation of gamma oscillation frequency by balancing excitation with inhibition. Neuron. 2009 May 28;62(4):566–77.

Bajaj V, Pachori RB. Classification of seizure and non-seizure EEG signals using empirical mode decomposition. IEEE Trans Inf Technol Biomed. 2012 Nov;16(6):1135–42.

Bartz S, Avarvand FS, Leicht G, Nolte G. Analyzing the waveshape of brain oscillations with bicoherence. Neuroimage. 2018 Nov;

Belluscio MA, Mizuseki K, Schmidt R, Kempter R, Buzsáki G. Cross-frequency phase-phase coupling between θ and γ oscillations in the hippocampus. J Neurosci. 2012 Jan 11;32(2):423–35.

Bruns A. Fourier-, Hilbert- and wavelet-based signal analysis: are they really different approaches? J Neurosci Methods. 2004 Aug 30;137(2):321–32.

Buzsáki G, Czopf J, Kondákor I, Kellényi L. Laminar distribution of hippocampal rhythmic slow activity (RSA) in the behaving rat: current-source density analysis, effects of urethane and atropine. Brain Res. 1986 Feb 12;365(1):125–37.

Buzsáki G, Rappelsberger P, Kellényi L. Depth profiles of hippocampal rhythmic slow activity ('theta rhythm') depend on behaviour. Electroencephalogr Clin Neurophysiol. 1985 Jul;61(1):77–88.

Canolty RT, Edwards E, Dalal SS, Soltani M, Nagarajan SS, Kirsch HE, et al. High gamma power is phase-locked to theta oscillations in human neocortex. Science. 2006 Sep 15;313(5793):1626–8.

Chandran K S S, Mishra A, Shirhatti V, Ray S. Comparison of Matching Pursuit Algorithm with Other Signal Processing Techniques for Computation of the Time-Frequency Power Spectrum of Brain Signals. J Neurosci. 2016 Mar 23;36(12):3399–408.

Cole SR, van der Meij R, Peterson EJ, de Hemptinne C, Starr PA, Voytek B. Nonsinusoidal beta oscillations reflect cortical pathophysiology in parkinson's disease. J Neurosci. 2017 May 3;37(18):4830–40.

Cole SR, Voytek B. Brain oscillations and the importance of waveform shape. Trends Cogn Sci (Regul Ed). 2017 Jan 4;21(2):137–49.

Cole SR, Voytek B. Hippocampal theta bursting and waveform shape reflect CA1 spiking patterns. BioRxiv. 2018 Oct 25.

Cole SR, Donoghue T, Gao R, Voytek B. NeuroDSP: A package for neural digital signal processing. 2019. Journal of Open Source Software.

Diez PF, Mut V, Laciar E, Torres A, Avila E. Application of the empirical mode decomposition to the extraction of features from EEG signals for mental task classification. Conf Proc IEEE Eng Med Biol Soc. 2009;2009:2579–82.

van Dijk H, van der Werf J, Mazaheri A, Medendorp WP, Jensen O. Modulations in oscillatory activity with amplitude asymmetry can produce cognitively relevant event-related responses. Proc Natl Acad Sci USA. 2010 Jan 12;107(2):900–5.

Dvorak D, Fenton AA. Toward a proper estimation of phase-amplitude coupling in neural oscillations. J Neurosci Methods. 2014 Mar 30;225:42–56.

Feingold J, Gibson DJ, DePasquale B, Graybiel AM. Bursts of beta oscillation differentiate postperformance activity in the striatum and motor cortex of monkeys performing movement tasks. Proc Natl Acad Sci USA. 2015 Nov 3;112(44):13687–92.

Fransen AMM, van Ede F, Maris E. Identifying neuronal oscillations using rhythmicity. Neuroimage. 2015 Sep;118:256–67.

Gao RD, Peterson EJ, Voytek B. Inferring synaptic excitation/inhibition balance from field potentials. 2017. NeuroImage 158: 70-78.

Gerber EM, Sadeh B, Ward A, Knight RT, Deouell LY. Non-Sinusoidal Activity Can Produce Cross-Frequency Coupling in Cortical Signals in the Absence of Functional Interaction between Neural Sources. PLoS ONE. 2016 Dec 12;11(12):e0167351.

Gips B, Bahramisharif A, Lowet E, Roberts MJ, de Weerd P, Jensen O, et al. Discovering recurring patterns in electrophysiological recordings. J Neurosci Methods. 2017 Jan 1;275:66–79.

Haller M, Donoghue T, Peterson E, Varma P, Sebastian P, Gao R, et al. Parameterizing neural power spectra. BioRxiv. 2018 Apr 11;

Hanslmayr S, Aslan A, Staudigl T, Klimesch W, Herrmann CS, Bäuml K-H. Prestimulus oscillations predict visual perception performance between and within subjects. Neuroimage. 2007 Oct 1;37(4):1465–73.

de Hemptinne C, Swann NC, Ostrem JL, Ryapolova-Webb ES, San Luciano M, Galifianakis NB, et al. Therapeutic deep brain stimulation reduces cortical phase-amplitude coupling in Parkinson's disease. Nat Neurosci. 2015 May;18(5):779–86.

Hentschke H, Perkins MG, Pearce RA, Banks MI. Muscarinic blockade weakens interaction of gamma with theta rhythms in mouse hippocampus. Eur J Neurosci. 2007 Sep;26(6):1642–56.

Hughes AM, Whitten TA, Caplan JB, Dickson CT. BOSC: a better oscillation detection method, extracts both sustained and transient rhythms from rat hippocampal recordings. Hippocampus. 2012 Jun;22(6):1417–28.

Jackson N, Cole SR, Voytek B, Swann NC. Characteristics of waveform shape in Parkinson's disease detected with scalp electroencephalography. eNeuro. 2019 May;6(3).

Jas M, Tour T, Şimşekli U, Re G. Learning the Morphology of Brain Signals Using Alpha-Stable Convolutional Sparse Coding. Arxiv. 2017;

Jones SR. When brain rhythms aren't "rhythmic": implication for their mechanisms and meaning. Curr Opin Neurobiol. 2016 Jul 9;40:72–80.

Klimesch W. EEG alpha and theta oscillations reflect cognitive and memory performance: a review and analysis. Brain Res Rev. 1999 Apr;29(2–3):169–95.

Kramer MA, Tort ABL, Kopell NJ. Sharp edge artifacts and spurious coupling in EEG frequency comodulation measures. J Neurosci Methods. 2008 May 30;170(2):352–7.

Latimer KW, Yates JL, Meister MLR, Huk AC, Pillow JW. NEURONAL MODELING. Single-trial spike trains in parietal cortex reveal discrete steps during decision-making. Science. 2015 Jul 10;349(6244):184–7.

Lee S, Jones SR. Distinguishing mechanisms of gamma frequency oscillations in human current source signals using a computational model of a laminar neocortical network. Front Hum Neurosci. 2013 Dec 18;7:869.

Lewis LD, Weiner VS, Mukamel EA, Donoghue JA, Eskandar EN, Madsen JR, et al. Rapid fragmentation of neuronal networks at the onset of propofol-induced unconsciousness. Proc Natl Acad Sci USA. 2012 Dec 4;109(49):E3377-86.

Liang H, Bressler SL, Desimone R, Fries P. Empirical mode decomposition: a method for analyzing neural data. Neurocomputing. 2005 Jun;65–66:801–7.

Lopes-Dos-Santos V, van de Ven GM, Morley A, Trouche S, Campo-Urriza N, Dupret D. Parsing Hippocampal Theta Oscillations by Nested Spectral Components during Spatial Exploration and Memory-Guided Behavior. Neuron. 2018 Nov 21;100(4):940–952.e7.

Lozano-Soldevilla D, Ter Huurne N, Oostenveld R. Neuronal Oscillations with Non-sinusoidal Morphology Produce Spurious Phase-to-Amplitude Coupling and Directionality. Front Comput Neurosci. 2016 Aug 22;10:87.

Massimini M, Huber R, Ferrarelli F, Hill S, Tononi G. The sleep slow oscillation as a traveling wave. J Neurosci. 2004 Aug 4;24(31):6862–70.

Mazaheri A, Jensen O. Rhythmic pulsing: linking ongoing brain activity with evoked responses. Front Hum Neurosci. 2010 Oct 14;4:177.

Mazzoni A, Linden H, Cuntz H, Lansner A, Panzeri S, Einevoll G. Computing the Local Field Potential (LFP) from Integrate-and-Fire Network Models. J Comput Biol. 2015 Dec 1:38.

Miller KJ, Leuthardt EC, Schalk G, Rao RPN, Anderson NR, Moran DW, et al. Spectral changes in cortical surface potentials during motor movement. J Neurosci. 2007 Feb 28;27(9):2424–32.

Nelli S, Itthipuripat S, Srinivasan R, Serences JT. Fluctuations in instantaneous frequency predict alpha amplitude during visual perception. Nat Commun. 2017 Dec 12;8(1):2071.

Orosco L, Laciar E, Correa AG, Torres A, Graffigna JP. An epileptic seizures detection

algorithm based on the empirical mode decomposition of EEG. Conf Proc IEEE Eng Med Biol Soc. 2009;2009:2651–4.

Park C, Looney D, Naveed ur Rehman, Ahrabian A, Mandic DP. Classification of motor imagery BCI using multivariate empirical mode decomposition. IEEE Trans Neural Syst Rehabil Eng. 2013 Jan;21(1):10–22.

Peterson EJ, Voytek B. Alpha oscillations control cortical gain by modulating excitatory-inhibitory background activity. BioRxiv. 2017 Sep 7.

Podvalny E, Noy N, Harel M, Bickel S, Chechik G, Schroeder CE, Mehta AD, Tsodyks M, Malach R. A unifying principle underlying the extracellular field potential spectral responses in the human cortex. Journal of Neurophysiology. 2015 Apr;114(1):505-519.

Pfurtscheller G, Stancák A, Edlinger G. On the existence of different types of central beta rhythms below 30 Hz. Electroencephalogr Clin Neurophysiol. 1997 Apr;102(4):316–25.

Pietersen ANJ, Patel N, Jefferys JGR, Vreugdenhil M. Comparison between spontaneous and kainate-induced gamma oscillations in the mouse hippocampus in vitro. Eur J Neurosci. 2009 Jun;29(11):2145–56.

Pittman-Polletta B, Hsieh W-H, Kaur S, Lo M-T, Hu K. Detecting phase-amplitude coupling with high frequency resolution using adaptive decompositions. J Neurosci Methods. 2014 Apr 15;226:15–32.

Ray S, Jouny CC, Crone NE, Boatman D, Thakor NV, Franaszczuk PJ. Human ECoG analysis during speech perception using matching pursuit: a comparison between stochastic and dyadic dictionaries. IEEE Trans Biomed Eng. 2003 Dec;50(12):1371–3.

Samaha J, Postle BR. The Speed of Alpha-Band Oscillations Predicts the Temporal Resolution of Visual Perception. Curr Biol. 2015 Nov 16;25(22):2985–90.

Sampson AL, Lainscsek C, Gonzalez CE, Ulbert I, Devinsky O, Fabó D, Madsen JR, Halgren E, Cash SS, Sejnowski TJ. Delay differential analysis for dynamical sleep spindle detection. *J Neurosci Methods. 2019;* 316:12-21.

Schaworonkow N, Nikulin VV. Spatial neuronal synchronization and the waveform of oscillations: implications for EEG and MEG. BioRxiv. 2018 Aug 27;

Scheffer-Teixeira R, Tort AB. On cross-frequency phase-phase coupling between theta and gamma oscillations in the hippocampus. elife. 2016 Dec 7;5.

Sherman MA, Lee S, Law R, Haegens S, Thorn CA, Hämäläinen MS, et al. Neural mechanisms of transient neocortical beta rhythms: Converging evidence from humans, computational modeling, monkeys, and mice. Proc Natl Acad Sci USA. 2016 Aug 16;113(33):E4885-94.

Siapas AG, Lubenov EV, Wilson MA. Prefrontal phase locking to hippocampal theta oscillations. Neuron. 2005 Apr 7;46(1):141–51.

Trimper JB, Stefanescu RA, Manns JR. Recognition memory and theta-gamma interactions in the hippocampus. Hippocampus. 2014 Mar;24(3):341–53.

Uhlhaas PJ, Singer W. Abnormal neural oscillations and synchrony in schizophrenia. Nat Rev Neurosci. 2010 Feb;11(2):100–13.

Vaz AP, Yaffe RB, Wittig JH, Inati SK, Zaghloul KA. Dual origins of measured phase-amplitude coupling reveal distinct neural mechanisms underlying episodic memory in the human cortex. Neuroimage. 2017 Mar 1;148:148–59.

Voytek B, D'Esposito M, Crone NE, Knight RT. A method for event-related phase/amplitude

coupling. NeuroImage. 2013 64: 416-424.

Voytek B, Knight RT. Dynamic network communication as a unifying neural basis for cognition, development, aging, and disease. Biol Psychiatry. 2015 Jun 15;77(12):1089–97.

Voytek B, Kayser A, Badre D, Fegen D, Chang EF, Crone NE, Parvizi J, Knight RT, D'Esposito M. Oscillatory dynamics coordinating human frontal networks in support of goal maintenance. Nature Neuroscience. 2015 18(9): 1318-1324.

Watrous AJ, Miller J, Qasim SE, Fried I, Jacobs J. Phase-tuned neuronal firing encodes human contextual representations for navigational goals. BioRxiv. 2017 Oct 12;

Womelsdorf T, Valiante TA, Sahin NT, Miller KJ, Tiesinga P. Dynamic circuit motifs underlying rhythmic gain control, gating and integration. Nat Neurosci. 2014 Aug;17(8):1031–9.

Acknowledgements

We thank Richard Gao, Tammy Tran, and Tom Donoghue for invaluable discussion and comments on the manuscript.

Grants

S.R.C. is supported by the National Science Foundation Graduate Research Fellowship Program and the University of California, San Diego Chancellor's Research Excellence Scholarship. B.V is supported by a Sloan Research Fellowship, the Whitehall Foundation (2017-12-73), and the National Science Foundation (1736028).

Disclosures

No conflicts of interest, financial or otherwise, are declared by the authors.

Author contributions

S.R.C. performed the research. S.R.C. and B.V. designed the research and wrote the paper.

Figure Legends

Figure 1. Approach for decomposing a neural signal into individual cycles. *A:* Example raw field potential recording from the CA1 layer of rat hippocampus. *B:* The raw signal is lowpass filtered at 40 Hz (4 times the oscillation frequency) to remove high frequencies while preserving underlying theta waveform shape. *C:* Zero-crossings are found after the signal has been bandpass filtered in the theta frequency range (4-10 Hz). *D:* Peaks and troughs are found in the lowpass filtered signal by finding the relative maxima and minima between the zero-crossings found in the theta-filtered signal *A*. *E:* Flank midpoints are determined by locating the time points at which the voltage is halfway between the adjacent peak and trough voltages. These points denote the boundaries between peak and trough. *F:* Demonstration of features computed for a single cycle. The amplitude of the cycle is defined as the average voltage difference between the trough and adjacent peaks (blue lines). The period is defined as the time between consecutive peaks (red and orange lines together). The rise-decay symmetry is computed as the fraction of the period that the cycle is in the rise phase (orange line). Similarly, the peak-trough symmetry is defined as the relative amount of a cycle (both green lines together) is comprised of the time between the rise midpoint and the subsequent decay midpoint (i.e., the peak, light green line). *G:* Table showing the values of each cycle feature for each cycle. Each row corresponds to a single cycle whose trough occurs in *A*-*E* at the time indicated by the "trough time" column.

Figure 2. Comparison of two simulated signals using a cycle-by-cycle approach. *A-F:* Two neural signals were simulated for 1000 seconds each. The first signal *A* was composed of a nonstationary oscillation (*B*) and aperiodic noise (*C*). The second signal *D* is simulated with a slightly larger oscillation (*E*) that is more asymmetric (rise shorter than decay) and slightly less aperiodic noise (*F*). *G-J:* Distributions of cycle features comparing the signals in *A* (black) and *D* (red). Compared to signal *A*, the cycles in *D* are generally (*G*) larger in amplitude, (*H*) have the same period, (*I*) are more asymmetric with a shorter rise, and, (*J*) are equally peak-trough symmetric. This shows, using ground-truth simulations, that the cycle-by-cycle approach successfully discriminates signals along the appropriate dimensions that differ.

Figure 3. Accuracy of measured cycle features in simulated signals with noise. *A-B*: Two simulated neural signals with relatively large amounts of noise (*A*, SNR = 0.32) and relatively low amounts of noise (*B*, SNR = 3.2). The ground-truth oscillation that was simulated (gray) is compared to the simulated "recording" used to compute cycle features (black). These simulated recordings are the result of adding noise to the ground-truth oscillation followed by application of a 40 Hz lowpass filter to aid in extrema localization. Note that this recovered oscillatory signal has substantial differences compared to the generated oscillation due to corruption from the added noise, particularly in *A*. *C-E:* Comparison between measured and ground-truth cycle features for the signal plotted in *A*. Each dot corresponds to 1 cycle for its measured and true *C* amplitude, *D* period, and *E* rise-decay symmetry. *F-H:* Same as *C-E* except for the signal plotted in *B*. Note the stronger correlations between measured and ground-truth cycle features. *I*: Average measurement error of individual cycle features for simulated signals with SNR ranging from 0.1 to 10.

Figure 4. Comparison of amplitude measurement methods on simulated event-related data. *A:* Three different event-related oscillatory changes were simulated for an event occurring at 0.0 seconds: (1, black) a "baseline" condition in which 10 Hz oscillations were randomly added to the data after a simulated event onset; (2, red) a "higher amplitude" condition in which the oscillations were 10% larger than in the "baseline" condition, and; (3, blue) a "more bursts" condition wherein oscillations were more common than the other conditions. While 1 example trial for each condition is shown, 100 trials were simulated for each condition. *B:* Event-related instantaneous amplitude profiles, using conventional approach of filtering and the Hilbert transform, were averaged across the three trial types in *A*. *C:* Same as *B*, but amplitude was estimated using the cycle-by-cycle approach. Amplitude estimates were binned at 100 ms intervals. *D:* Same as *C*, but showing the probability of an oscillation being detected for each condition, binned at 100 ms intervals. Note that this measure is not a standard output for conventional analyses. *E-F:* Distributions of the average *E* instantaneous amplitude and *F* cycle amplitude between 500 ms and 1000 ms for each trial in the "baseline" (black) and "higher amp" (red) conditions. Note that the instantaneous amplitude measure did not significantly differentiate the amplitude across these two conditions ($p = 0.10$). In contrast, the cycle-by-cycle amplitude estimate accurately shows that the amplitude is greater in the "higher amp" condition compared to the "baseline" condition ($p < 10^{-5}$). *G-H:* Similar to *E-F* but showing the difference in amplitude distributions between the "baseline" (black) and "more bursts" (blue) conditions. Note that the instantaneous amplitude estimates are larger in the "more bursts" condition ($p < 10^{-7}$), while the cycle-by-cycle amplitude estimate is relatively unchanged ($p = 0.37$).

Figure 5. Comparison of frequency estimation methods on simulated event-related data. *A:* Three different event-related oscillatory changes were simulated for an event occurring at 0.0 seconds: (1, black) a "baseline" condition in which 10 Hz oscillations were randomly added to

the data after a simulated event onset; (2, red) a “faster” condition in which the oscillations were simulated at 11 Hz, and; (3, blue) a “more bursts” condition wherein oscillations were more common than in the other conditions. While 1 example trial for each condition is shown, 100 trials were simulated for each condition. *B:* Event-related instantaneous frequency profiles, using conventional approach of filtering and the Hilbert transform, were averaged across the three trial types in *A*. *C:* Same as *B*, but frequency was estimated using the cycle-by-cycle approach. Frequency estimates were binned at 100 ms intervals. *D-E:* Distributions of the average *D* instantaneous frequency and *E* cycle-by-cycle frequency estimate between 500 ms and 1000 ms for each trial in the “baseline” (black) and “faster” (red) conditions. Note that both the instantaneous and cycle-by-cycle frequency measures differentiated these conditions ($p < 10^{-4}$). Also note that the cycle-by-cycle frequency distributions were accurately around 10 Hz for the “baseline” condition and 11 Hz for the “faster” condition, while the instantaneous frequency measures were often estimated to be lower than the ground-truth simulation. *F-G:* Similar to *D-E* but showing the difference in frequency distributions between the “baseline” (black) and “more bursts” (blue) conditions. Note that the instantaneous frequency estimates are higher in the “more bursts” condition (*F*, $p < 10^{-4}$), while the cycle-by-cycle frequency estimate is appropriately unchanged (*G*, $p = 0.45$).

Figure 6. Changes in motor cortical beta oscillation shape with deep brain stimulation (DBS) treatment of Parkinson’s disease. *A-B:* Motor cortical electrocorticography recordings from one subject *A*, before, and *B*, during, DBS.*C-F:* Comparison of *C* amplitude, *D* period, *E* rise-decay symmetry, and *F* peak-trough symmetry of beta oscillations in the same subject before (black) and during (red) DBS. *G:* Comparison of peak-trough asymmetry of beta oscillations before and during DBS. This value is computed as the absolute difference between the peak-trough symmetry and 0.5 (equal peak and trough duration). Each dot represents one subject. The diagonal line represents the same peak-trough asymmetry before and during DBS. These results replicate previous work showing that peak-trough asymmetry is reduced during DBS treatment in most patients, in this case using methods that focus only on recording segments in an oscillation.

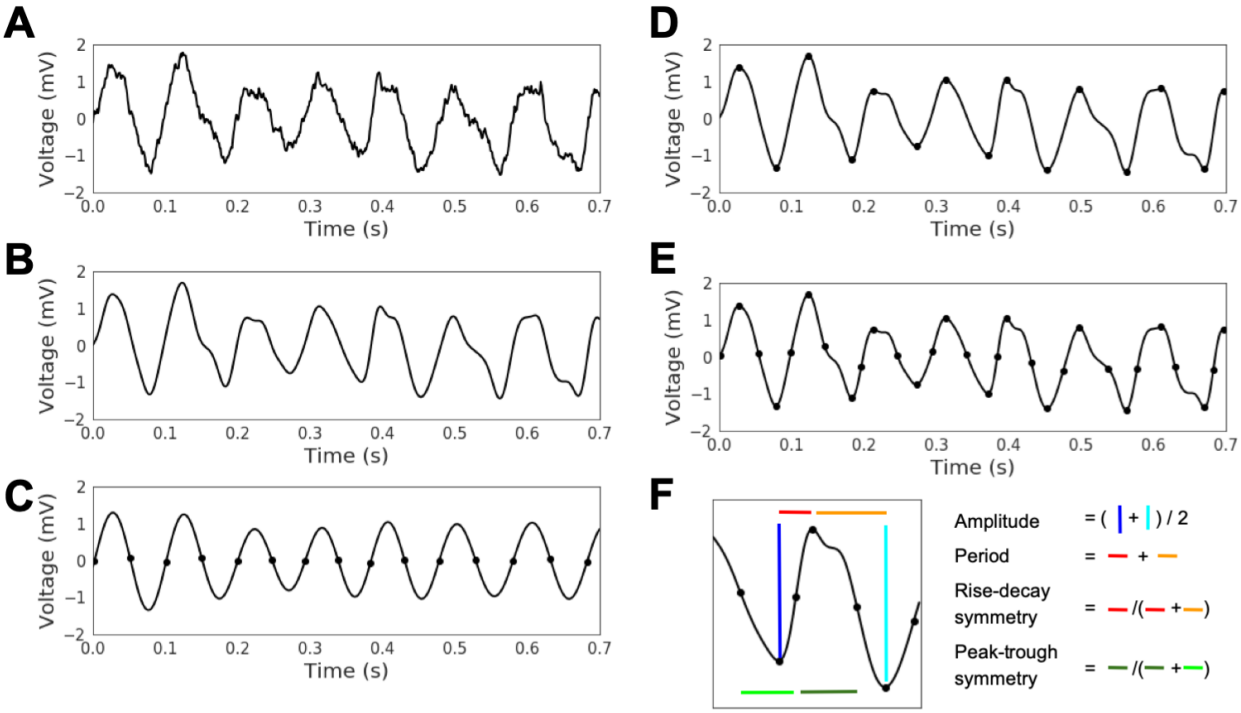

G

Peak time	Amplitude	Period	rdsym	ptsym
0.12	2.9	105	0.43	0.51
0.21	1.7	89	0.34	0.5
0.31	1.9	99	0.4	0.49
0.4	2.2	82	0.32	0.52
0.5	2.2	109	0.4	0.58
0.61	2.2	108	0.44	0.57

Fig. 1

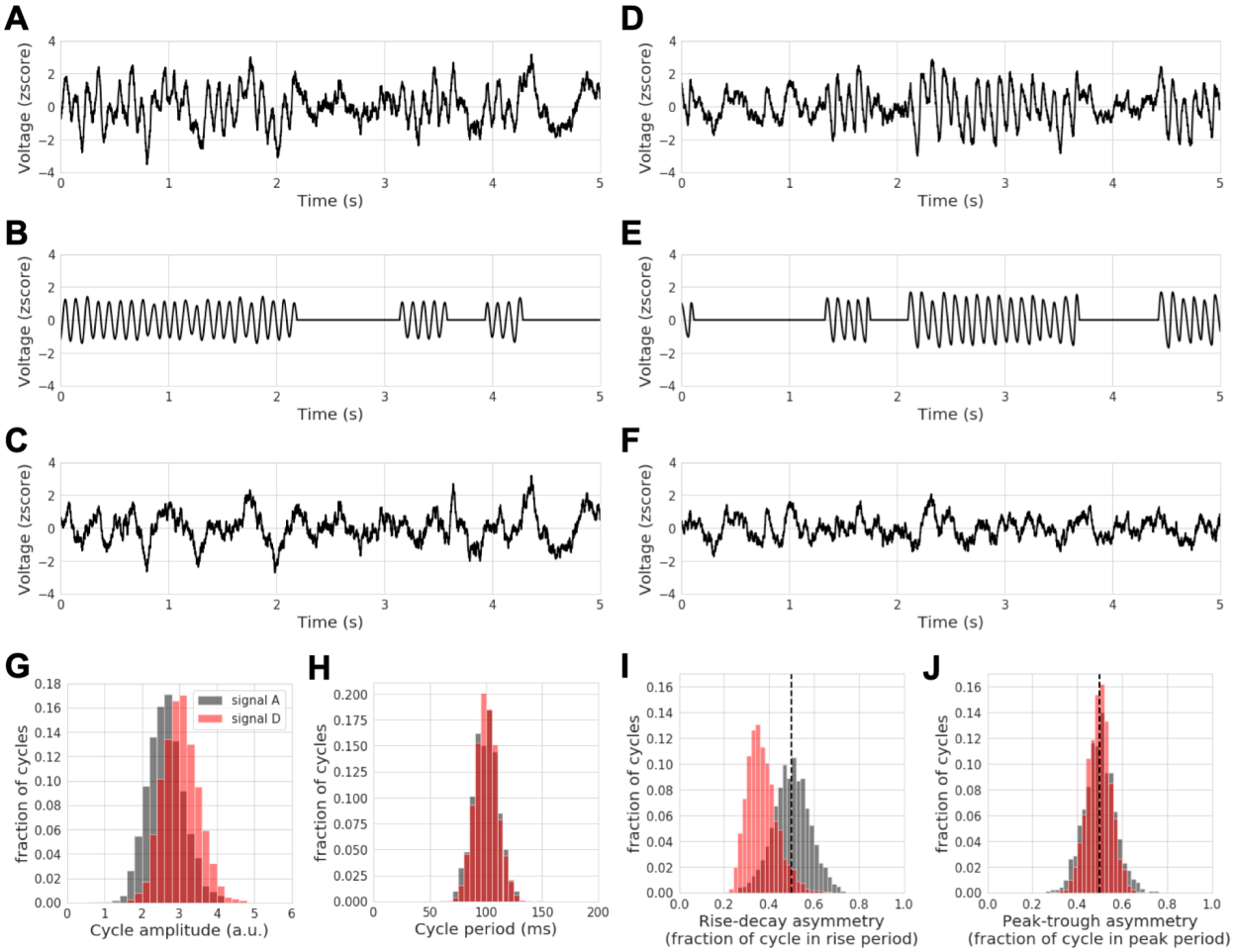
A
B
C
D
E
F
G
H
I
J
Voltage (zscore)
Time (s)
signal A
signal D
fraction of cycles
Cycle amplitude (a.u.)
Cycle period (ms)
Rise-decay asymmetry
(fraction of cycle in rise period)
Peak-trough asymmetry
(fraction of cycle in peak period)

Fig. 2

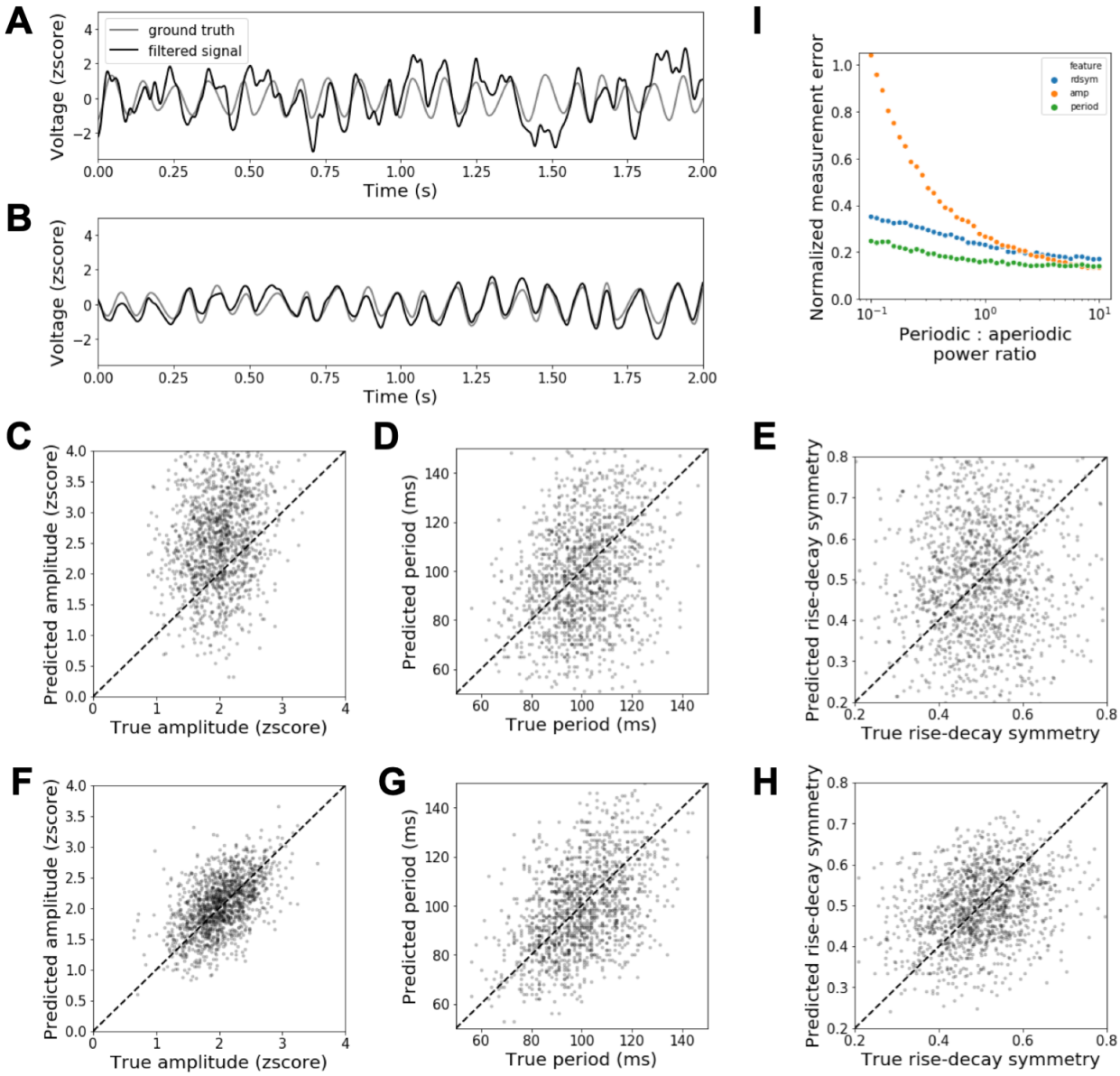
A
ground truth
filtered signal
Voltage (zscore)
Time (s)
B
Voltage (zscore)
Time (s)
I
feature
rdsym
amp
period
Normalized measurement error
Periodic : aperiodic
power ratio
C
Predicted amplitude (zscore)
True amplitude (zscore)
D
Predicted period (ms)
True period (ms)
E
Predicted rise-decay symmetry
True rise-decay symmetry
F
Predicted amplitude (zscore)
True amplitude (zscore)
G
Predicted period (ms)
True period (ms)
H
Predicted rise-decay symmetry
True rise-decay symmetry

Fig. 3

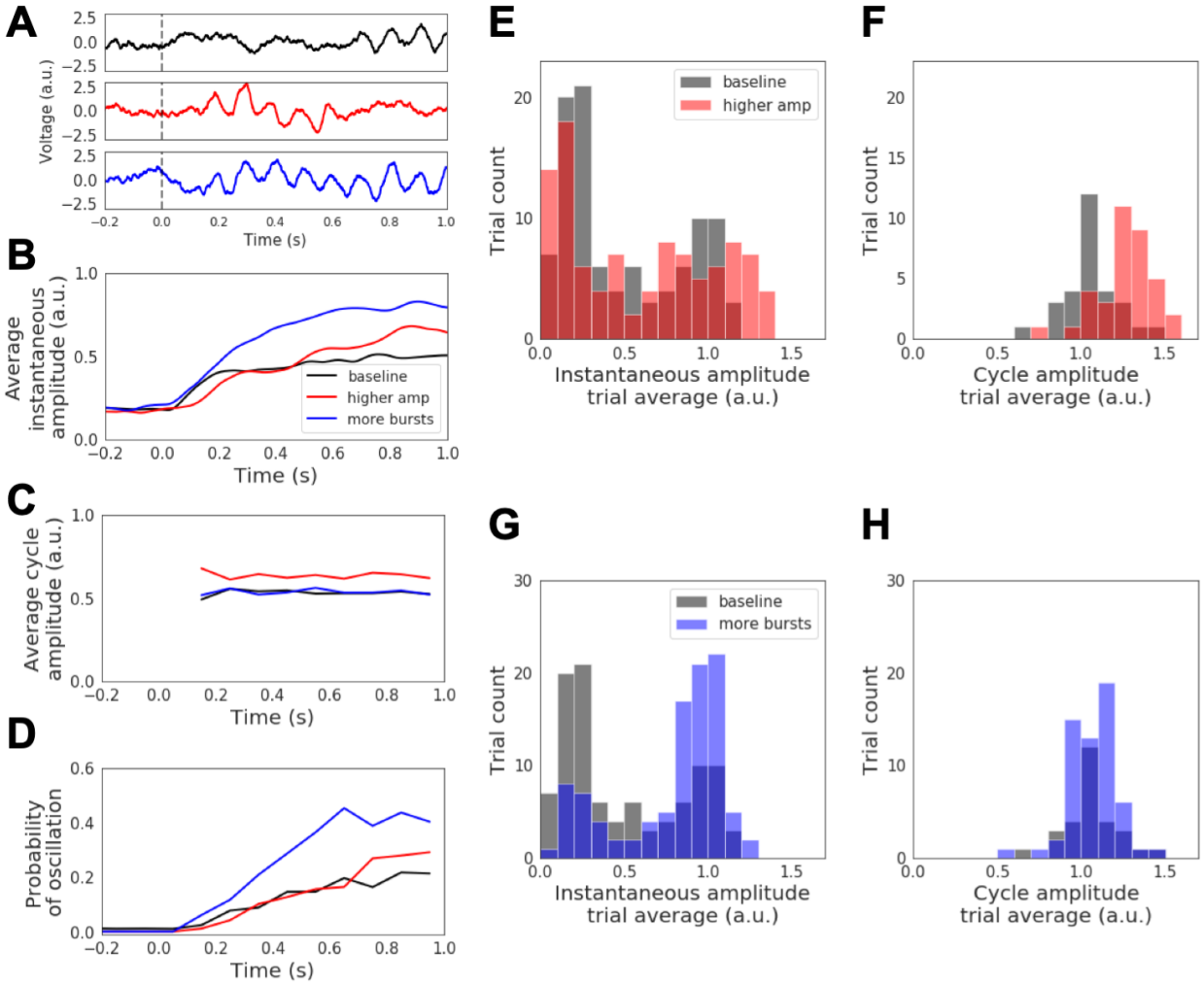
A
Voltage (a.u.)
Time (s)
B
Average instantaneous amplitude (a.u.)
baseline
higher amp
more bursts
Time (s)
C
Average cycle amplitude (a.u.)
Time (s)
D
Probability of oscillation
Time (s)
E
Trial count
baseline
higher amp
Instantaneous amplitude trial average (a.u.)
F
Trial count
Cycle amplitude trial average (a.u.)
G
Trial count
baseline
more bursts
Instantaneous amplitude trial average (a.u.)
H
Trial count
Cycle amplitude trial average (a.u.)

Fig. 4

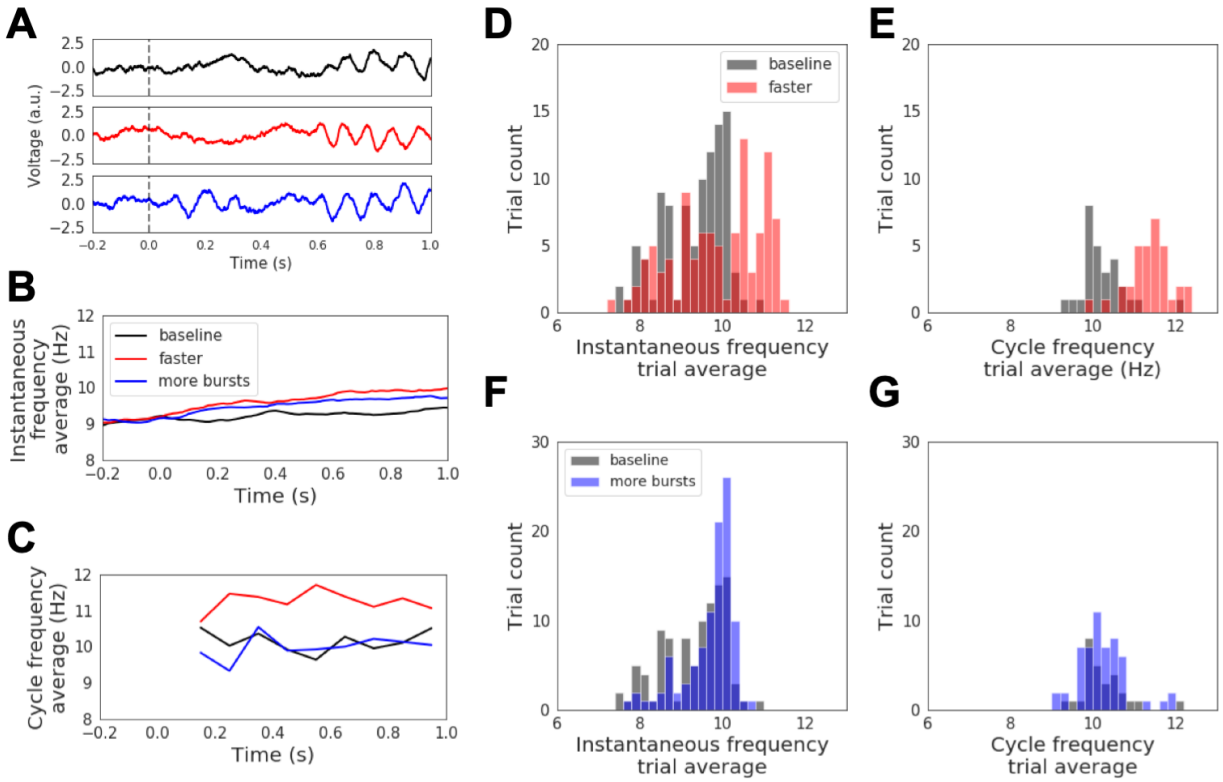
A
Voltage (a.u.)
Time (s)
B
Instantaneous frequency average (Hz)
baseline
faster
more bursts
Time (s)
C
Cycle frequency average (Hz)
Time (s)
D
Trial count
baseline
faster
Instantaneous frequency trial average
E
Trial count
Cycle frequency trial average (Hz)
F
Trial count
baseline
more bursts
Instantaneous frequency trial average
G
Trial count
Cycle frequency trial average

Fig. 5

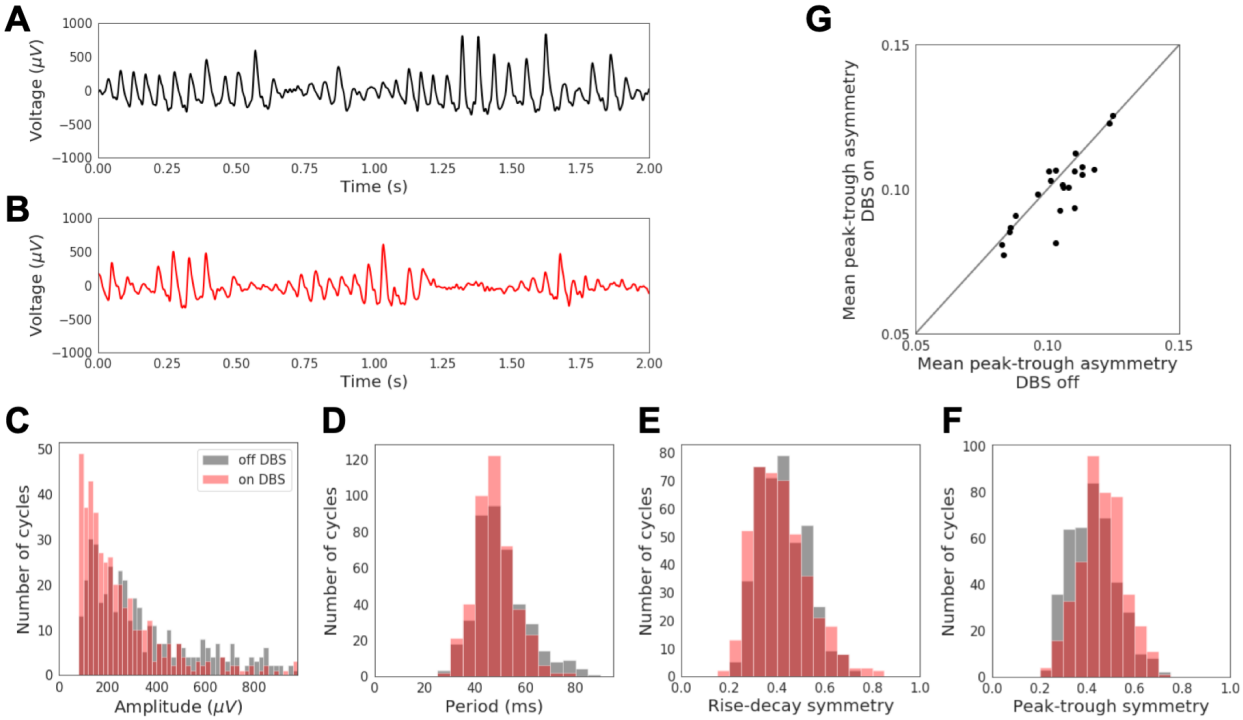
A
Voltage (μV)
Time (s)
B
Voltage (μV)
Time (s)
G
Mean peak-trough asymmetry DBS on
Mean peak-trough asymmetry DBS off
C
off DBS
on DBS
Number of cycles
Amplitude (μV)
D
Number of cycles
Period (ms)
E
Number of cycles
Rise-decay symmetry
F
Number of cycles
Peak-trough symmetry

Fig. 6